Characterization of nanocrystalline NiCuZn ferrite powders synthesized by sol-gel auto-combustion method

P.K. Roy, J. Bera*
Department of Ceramic Engineering,
National Institute of Technology, Rourkela-769008, INDIA

Published in

Journal of Materials Processing Technology

Volume 197, Issues 1-3, 1 February 2008, Pages 279-283

http://dx.doi.org/10.1016/j.jmatprotec.2007.06.027

*Corresponding author. Tel.: +91 9437246159
Fax: +91 661 2472926.
E-mail address: jbera@nitrkl.ac.in,jbera@rediffmail.com

Abstract

The ferrite compositions $Ni_{0.8-x}Cu_{0.2}Zn_xFe_2O_4$ with x=0.5, 0.55 and 0.6, were synthesized through nitrate-citrate gel auto-combustion method. The autocatalytic nature of the combustion process has been studied by thermal analysis (DTA & TG) of the dried gels. The powders were calcined at 700°C/2h and then pressed ferrite parts were sintered at 900°C/4h. The ferrite was characterized with respect to phase identification, crystallite size and lattice parameter determination using X-ray diffraction. As-burnt powders showed the presence of crystalline cubic spinel ferrite with about 19-22 nm crystallite sizes. The densification characteristic of the powder was investigated using TMA. The sintered ferrite was characterized for permeability, saturation magnetization, relative loss and AC resistivity measurements. The permeability and magnetization were found to increase and magnetic loss, AC resistivity were decreased with Zn substitution for Ni. The powder is suitable for the application in multilayer chip inductor due to its low temperature sinterability, good magnetic properties and low loss at high frequency.

Keywords: A. Ceramics; B. magnetic materials; C. electrical properties; D. magnetic properties.

1. Introduction

Multilayer Chip Inductor (MLCI) is a passive surface mount device (SMD) widely used in electronic products, such as cellular phone, notebook computer and video cameras [1-2]. MLCIs are produced by co-firing ferrite layers with an internal silver conductor. NiCuZn ferrites have been the dominant ferrite materials for MLCI due to its better magnetic properties at high frequency and low sintering temperature [3-5]. Since silver (internal conductor) has a melting point of 961°C, a much lower (<961°C) sintering temperature of ferrite is preferred to suppress the diffusion of silver metal into the ferrite core. This metal diffusion into the ferrite body decreases the resistivity of core. The sintering temperature of the ferrite can

be decreased by using fine powder (small grain size and reactive). That is why the synthesis of fine reactive ferrite powder is one of the most important steps in MLCI technology. It is well known that the ultrafine powder can be prepared through various wet-chemical methods like co-precipitation, hydrothermal synthesis and sol-gel processes [6-8]. Although the co-precipitation and sol-gel methods are the most popular, they have some disadvantages. Most of the co-precipitation processes are highly pH sensitive and require special attention for complex systems like NiCuZn whereas the sol-gel technique requires expensive alkoxide precursor material and stringent process of gel product. The sol-gel auto combustion method, used here, has much simple processing steps. It has the advantages of using inexpensive precursors and low external energy consumption by the use of auto combustion process. The synthesis also results in the formation of nano-sized, homogeneous and highly reactive powder [9].

The various compositions of the system $Ni_{1-x-y}Zn_xCu_yFe_2O_4$ were investigated and reported in the literature [2-5, 9, 11, 12 and 15]. However, the reports on the specific composition system $Ni_{0.8-x}Cu_{0.2}Zn_xFe_2O_4$ with x=0.5, 0.55 and 0.6, is not available in the literature. In the present study, these ferrite compositions were investigated. The Zn substitution in this range x=0.5 to 0.6 were used as the saturation magnetization were reported to be maximized in that range for other ferrites [10]. The Cu content of the compositions was kept constant at 20 atom% of A site (AB_2O_4 spinel), because the DC resistivity was maximized near that composition [11]. The nitrate-citrate gel combustion was used to synthesize nano-crystalline, ferrite powder. The sinterability of the powder, electro-magnetic properties and magnetization of sintered ferrite were investigated with respect to Zn substitution for Ni in the spinel structure.

2. Experimental

Analytical grade Nickel Nitrate [$Ni(NO_3)_2.6H_2O$], Zinc Nitrate [$Zn(NO_3)_2.\ 6H_2O$], Copper Nitrate [$Cu(NO_3)_2.3H_2O$], Iron Nitrate [$Fe(NO_3)_3.\ 9H_2O$] and Citric Acid [$C_6H_8O_7.H_2O$] were used to prepare the ferrite compositions $Ni_{0.8-x}Cu_{0.2}Zn_x\ Fe_2O_4$ with x=0.5, 0.55, 0.6. Metal nitrates and citric acid were

dissolved in deionized water. Nitrate solutions were standardized through chemical analysis using ethylenediamine tetraacetic acid (EDTA) complexometric titration. Nitrate and citric acid solutions were mixed in 1:1 molar ratio of nitrates to citric acid. The pH of the solution was adjusted to 7 using ammonia solution. Then the solution was heated at 80ºC to transform into gel. When ignited at any point of the gel, the dried gel burnt in a self-propagating combustion manner until all gels were completely burnt out to form a fluffy loose powder. The auto-ignition of gel was carried out in BOROSIL glass beaker upon a hot plate. The autocatalytic nature of the combustion process has been studied by Differential Thermal Analysis (DTA) and thermogravimetry (TG) analysis of the dried gels.

The as burnt ash was calcined at 700^{o}C/2h for better crystallization and homogeneous cation distribution in the spinal. As the auto combustion rate is so rapid that the cations may not be well distributed in ferrite lattice of as-burnt ashes. Also it has been reported that the calcined material exhibits good crystallinity and optimum magnetic properties [12]. The calcined ferrite powder was granulated using polyvinyl alcohol as a binder and was uniaxially pressed at a pressure of 2 ton/cm^2 to form toroidal and pallet specimens. The specimens were sintered at 900^{0}C for 4hr in air atmosphere. The sintering behavior of the synthesized powder was evaluated by thermal mechanical analysis (TMA, Netzsch DIL 402C, Germany). The bulk density and apparent porosity of sintered ferrites was measured by Archimedes principle.

The as-burnt ash, calcined powders and the sintered ferrites were characterized with respect to phase identification, crystallite size and lattice parameter determination using X-ray diffraction (PW-1830, Philips, Netherlands) with Cu-Kα radiation. The crystallite size was calculated from peak broadening using Scherrer formula ($D_{hkl} = 0.9\lambda/\beta\text{Cos}\theta$), where D_{hkl} is the crystallite size perpendicular to (*hkl*) plane, λ is the wave length of X-ray used, β (rad) is the width of the diffraction peak and θ is the peak position. The full width at half maxima (FWHM) was used for β and it is expressed as β = B-b, where B and b (instrumental broadening) are FWHM for sample and Si standard, respectively. Fully crystalline Si metal standard pellet,

supplied with the Philips XRD system for calibration of the instrument, was used to measure the instrumental broadening (b) parameter.

The Impedance Analyzer (Hewlett Packard, Model 4192A, USA) was used to measure the inductance and the magnetic loss factor on toroids, wound with low capacitive 6 turns enameled copper wire. The resistivity was measured on pallet samples by applying silver electrodes on the surfaces.

Saturation magnetization measurement was carried out at room temperature using a vibrating sample magnetometer (VSM) (Lakeshore-7040) with a maximum magnetic field of 20kOe.

3. Results & Discussion

The experimental observation reveled that the nitrate-citrate gels exhibited self-propagating combustion behavior. Fig. 1 shows the DTA and TG of the dried gel. The DTA endothermic peak at about 140^{o}C may be due to the removal of residual water from gel. This dehydration process also produces a TG weight loss in the region 90-180^{o}C. The DTA exothermic peak at around 186^{o}C, associated with the second major TG weight loss, may be caused by the autocatalytic anionic oxidation-reduction reaction of nitrates with citric acid. This auto-combustion initiates the formation of NiCuZn ferrite through the solid-state diffusion process [13]. The nitrate-citrate combustion reaction (for example x= 0.6 composition) is as follows:

$$0.2\ Ni(NO_3)_2 + 0.2\ Cu(NO_3)_2 + 0.6\ Zn(NO_3)_2 + 2\ Fe(NO_3)_3 + 3C_6H_8O_7 \longrightarrow Ni_{0.2}Cu_{0.2}Zn_{0.6}Fe_2O_4 + 4N_2 + 18CO_2 + 12H_2O$$

The XRD patterns of as-burnt ferrite powders are shown in Fig. 2. The figure shows that the ferrites formed are in crystalline state and contain cubic spinel ferrite phases similar to JCPDS card No. 48-0489, with chemical composition: $Ni_{0.65}Cu_{0.1}Zn_{0.35}\ Fe_{1.9}O_4$, space group: F, and cell parameter a: 8.446 Å. No second phase was detected by XRD. The broad peaks in the XRD patterns indicate fine crystallite size of the ferrite particles. The crystallite size was calculated from peak broadening of (311) peak. The crystallite size of as

burnt ferrite powders was in the range 19-22 nm. This observation reveals that the nanocrystalline NiCuZn ferrite powders can be synthesized directly by the auto-combustion of nitrate- citrate gels.

The calcined and sintered ferrites were also characterized by XRD. As per expectation the crystallite size increases with successive heat treatment of the ferrite. Fig. 3 shows the diffraction pattern of as-burnt, calcined and sintered ferrite (for x=0.6 composition). The figure shows that the broadening of diffraction peak decreases from as-burnt –to-calcined –to- sintered product respectively. The crystallite sizes of calcined and sintered ferrites were in the range 37-39 and 80-145 nm respectively. The crystallite size of sintered product was very much dependant on the Zn concentration and that increases with Zn content (Table1). However, there was no or little influence of Zn on the crystallite size of as-burnt as well as calcined powders. The crystallite sizes of sintered ferrites are shown in Table 1, along with their bulk density, percent porosity, lattice parameter, permeability, saturation magnetization and resistivity. The bulk density increases with increasing Zn content, indicating improved densification by the addition of Zn in place of Ni. The same type of phenomena was observed in NiZn ferrite [14]. To see the effect of this Zn addition upon densification, sintering kinetics was also evaluated by TMA. Fig. 4 shows the shrinkage curves (5^{o}C/min heating rate in air) of different ferrite samples. The figure shows that the slope of the shrinkage curve decreases with decreasing Zn content. This indicates that the rate of densification decreases with the decreases in Zn content. It has been reported that the densification process of NiCuZn ferrite slows down in presence of large quantity of NiO [15]. From the present study it may be concluded that densification rate of the ferrite increases with the Zn substitution or by the decrease in NiO content. The crystallite size of the sintered ferrite was also found to increase with the increase in Zn substitution. This indicates that the Zn plays an important role during sintering of the ceramics. It is also evident from the Fig. 4 that the sintering temperature ($\approx 900^{o}$C) of the ferrite, is much lower than that ($>1100^{o}$C) of powders prepared by the conventional solid state reaction method [16]. The lattice parameter (Table 1) was found to

increase with increasing Zn^{+2} substitution of the ferrite. This is attributed to the larger ionic radius of Zn^{+2} (0.84Å) as compared to the Ni^{+2} (0.74 Å).

The permeability of the ferrite increases with the increase in Zn (x) content (Table 1). Fig. 5 also shows the same behavior. The similar increased magnetization was found (Fig. 6) with the increase in Zn substitution. The permeability and saturation magnetization were highest at the substitution x=0.6 (Table 1). The increase in permeability/magnetization may be primarily due to the substitution of nonmagnetic Zn ion (d^{10}) for Ni into the magnetic ferrite lattice. Zn^{+2} has a stronger preference for the tetrahedral site (A site), while Ni^{+2} ions (for which Zn is substituted) are located on octahedral site (B site) of AB_2O_4 spinel ferrite. Thus, Zn displaces Fe^{+3} from A to B site. As the magnetic spin of neighboring A and B-sites are anti-ferromagnetically coupled (due to the super exchange interaction in ferrite lattice), the net result is an increase in magnetic moment on the B sub-lattice, as well as the net magnetic moment of the crystal increases. The second reason may be attributed to the increase in bulk density and average crystallite size of the ferrite with increased Zn substitution. It is known that ferrites with higher density and larger average grain size possess a higher initial permeability. An increase in the density (decrease in porosity) of ferrites not only results in the reduction of demagnetizing field due to decreased porosity but also raises the spin rotational contribution, which in turn increases the permeability [17]. Fig. 5 also shows the frequency dependency of permeability of different $Ni_{0.8-x}Cu_{0.2}Zn_xFe_2O_4$. It shows that the permeability of compositions with x=0.5 and 0.55 are stable upto 10MHz, whereas that of the x=0.6 composition is stable only upto about 3MHz. The permeability of the same increases, i.e the dispersion occurs above about 3 MHz. That is due to the much higher permeability of the composition (x=0.6) compared to other two(x=0.5, 0.55). This can be explained by Snock's law that cut-off frequency is inversely proportional with magnetic permeability.

Fig. 7 shows the relative loss factor (RLF) i.e. the ratio of the magnetic loss tangent (tanδ) to initial permeability. High μ and low tanδ i.e. low RLF is required for high frequency magnetic applications. The

figure shows that the RLF decreases with Zn-substitution. That may be due to the better densification of the ferrite with the Zn addition. All ferrites have higher RLF at lower frequency (kHz) range, may be due to higher hysteresis losses arising from their porous structure (percent porosity; Table 1). It is known that hysteresis losses increase with the increase in porosity [18]. The RLF stabilizes in the MHz zone. The increase in RLF for composition x=0.6 after 3-4 MHz is due to the resonance-relaxation losses [19]. So it may be concluded that this composition is the best material to be used up to 4MHz applications.

Electrical resistivity is an important property of low temperature sintered ferrite for MLCI application. A small decrease in resistivity was found with increasing Zn content as shown in Table 1, as well as in Fig. 8. The decrease in resistivity with Zn substitution may be due to the increase in crystallite size (Table 1). It may be considered that under an ideal situation the crystallite size should corresponds to the grain size in the ceramic. So, it may be considered that grain size also increases with Zn substitution. The smaller grains result in large number of grain boundaries in the ceramics. Grain boundaries are highly dislocated areas. Imperfections, such as porosity, dislocations and other second phases are trapped in the grain boundaries. That's why it acts as scattering center for the flow of electrons and therefore grain boundaries are highly resistive [5]. Fig. 8 also shows the frequency dependency of AC resistivity for different compositions. The resistivity of all the compositions decreases with the increase in frequency. The AC resistivity (ρ) was calculated using the formula $\rho=1/(\omega\epsilon_0 k' \tan\delta)$, where, ϵ_0 is the permittivity of free space, k' is the relative dielectric constant, $\tan\delta$ is dissipation factor, ω is the angular frequency. The resistivity decreases with the increase in frequency due to the inverse relationship between them.

4. Conclusions

From this investigation it may be concluded that nano-crystalline NiCuZn ferrite can be synthesized by auto combustion of nitrate-citrate gel. In this work Zn has been substituted for Ni to study the effect of substitution. Zn substitution helps in better densification of the ferrite. The sinterability of combustion

synthesized powder (≈900°C) is much better than that of conventional solid-oxide route powder. The composition $Ni_{0.8}Cu_{0.2}Zn_{0.6}Fe_2O_4$ shows highest permeability, magnetization and lower loss factor among all the compositions studied here. The composition is highly suitable for application up to 4MHz frequency. Considering all the advantages, especially sinterability below 960°C, the composition may be suggested as a better material for MLCI applications.

Acknowledgements

Author, J. Bera wishes to thank Department of Science & Technology, Govt. of India, New Delhi, for providing financial support through project grant (Grant no. SR/S3/ME/04/2002-SERC-Engg).

References

[1] X. Qi , J. Zhou, Z. Yue et al., Key Eng. Mater. 593 (2002) 224.

[2] B. Li, Z. X. Yue, X. W. Qi, J. Zhou, Z. L. Gui, L.T. Li, Mat. Sci. Engg. B 99 (1-3) (2003) 252.

[3] T. Nakamura, J. Magn. Magn. Mater. 168 (1997) 285.

[4] J. H. Jean, C. H. Lee, W. S. Kou, J. Am. Ceram. Soc. 82 (2) (1999) 343.

[5] K. O. Low, F. R. Sale, J. Magn. Magn. Mater. 246 (2002) 30.

[6] V. V. Pankov, M. Pernet, P. Germi, P. Mollard, J. Magn. Magn. Mater. 120 (1993) 69.

[7] P. S. A. Kumar, J. J. Shrotri, C. E. Deshpande, J.Appl. Phys. 81 (1997) 4788.

[8] A. Dias, R. L. Moreira, N. D. S. Mohallen, J. Magn. Magn. Mater. 172 (1997) L9.

[9] Z. Yue, L. Li, J. Zhou, H. Zhang, Z. Gui, Mat. Sci. Engg. B 64 (1999) 68.

[10] J. Smit, H.P.J. Wijn, Ferites, (John Wiley & Sons, New York, 1959)

[11] J. H. Nam, H. H. Jung, J. Y. Shin, J. H. Oh, IEEE Trans. on Mag. 31 (1995 Nov) No. 6.

[12] Y. P. Fu, K. Y. Pan, C.H. Lin, Mat. Letters 57 (2002) 291.

[13] N. S. Gajbhiye, U. Bhattacharya, V. S. Darshane, Thermochim. Acta 264 (1995) 219.

[14] P. Yadoji, R. Peelamedu, D. Agrawal, R. Roy, Mat. Sci. Engg. B 98 (2003) 269.

[15] K. O. Low, F. R. Sale, J. Magn. Magn. Mater. 256 (2003) 221.

[16] G. L. Sun, J. B. Li, J. J. Sun, X. Z. Yang, J. Magn. Magn. Mater. 281 (2004) 173.

[17] J. J. Shrotri, S. D. Kulkarni, C. E. Deshpande, S. K. Dtate, Mater. Chem. Phys. 59 (1999) 1.

[18] L. Neel, Physica 15 (1949) 225–234.

[19] J. Bera, P. K. Roy, Physica B 363 (2005) 128.

Figure Caption:

Fig. 1. DTA/TG plots for the dry nitrate-citrate gel at 10^{o}C /min heating rate in air.

Fig. 2. XRD patterns of as-burnt powder of $Ni_{0.8-x}Cu_{0.2}Zn_xFe_2O_4$ ferrite with different Zn(x) content.

Fig. 3. XRD patterns of as-burnt, calcined and sintered $Ni_{0.2}Cu_{0.2}Zn_{0.6}Fe_2O_4$ ferrite

Fig. 4. Shrinkage curve at 5°C/min heating rate in air for $Ni_{0.8-x}Cu_{0.2}Zn_x\ Fe_2O_4$ ferrite with different Zn(x) content.

Fig. 5. Frequency dependency of permeability in $Ni_{0.8-x}Cu_{0.2}Zn_x\ Fe_2O_4$ ferrite with different Zn(x) content.

Fig. 6. Magnetic hysteresis curve for $Ni_{0.8-x}Cu_{0.2}Zn_x\ Fe_2O_4$ ferrite with different Zn(x) content measured by VSM at 20 kOe and room temperature.

Fig. 7. Relative loss factor as a function of frequency in $Ni_{0.8-x}Cu_{0.2}Zn_x\ Fe_2O_4$ ferrite with different Zn(x) content.

Fig. 8. AC resistivity as a function of frequency in $Ni_{0.8-x}Cu_{0.2}Zn_x\ Fe_2O_4$ ferrite with different Zn(x) content.

Table 1

Bulk density, percent porosity, lattice parameter, crystallite size, permeability, saturation magnetization and resistivity of sintered $Ni_{0.8-x}Cu_{0.2}Zn_x\ Fe_2O_4$ with different Zn(x) content.

(Zn-Content) "x"	Bulk Density (gm/cc)	Percentage Porosity	Lattice Parameter (Å)	Crystallite Size (nm)	Permeability (μ)	Saturation Magnetization (emu/g)	Resistivity (ohm-cm) at 100kHz
x= 0.5	4.46	17	8.405	81.85	45.48	63.56	$10.39*10^6$
x= 0.55	4.75	11	8.429	92.73	67.75	65.13	$8.9*10^6$
x= 0.6	4.93	7	8.438	142.84	126.84	68.13	$3.3*10^6$

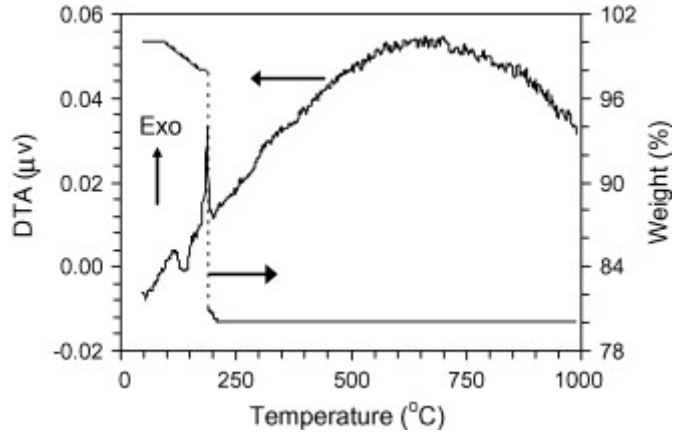

Fig. 1. DTA/TG plots for the dry nitrate–citrate gel at 10 °C/min heating rate in air.

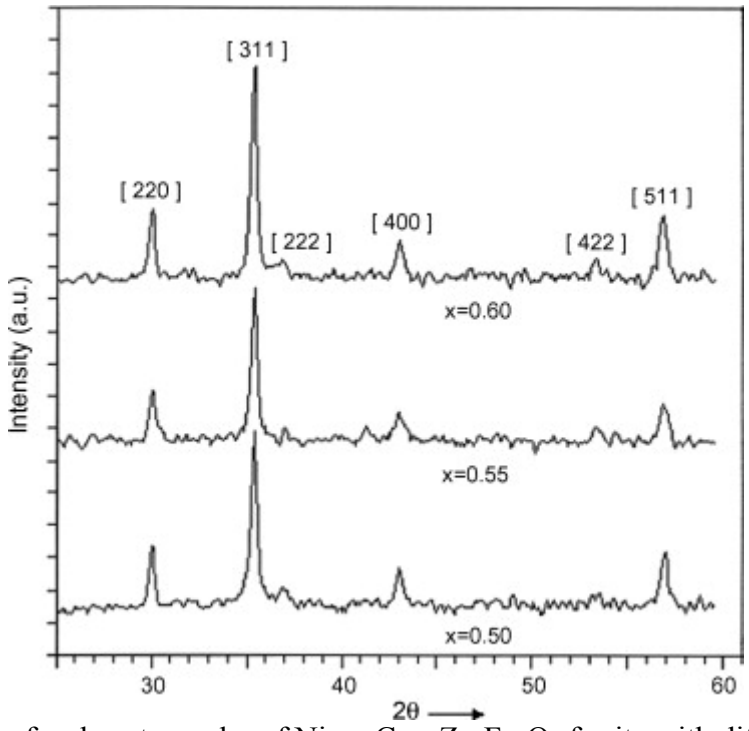

Fig. 2. XRD patterns of as-burnt powder of $Ni_{0.8-x}Cu_{0.2}Zn_xFe_2O_4$ ferrite with different Zn(x) content.

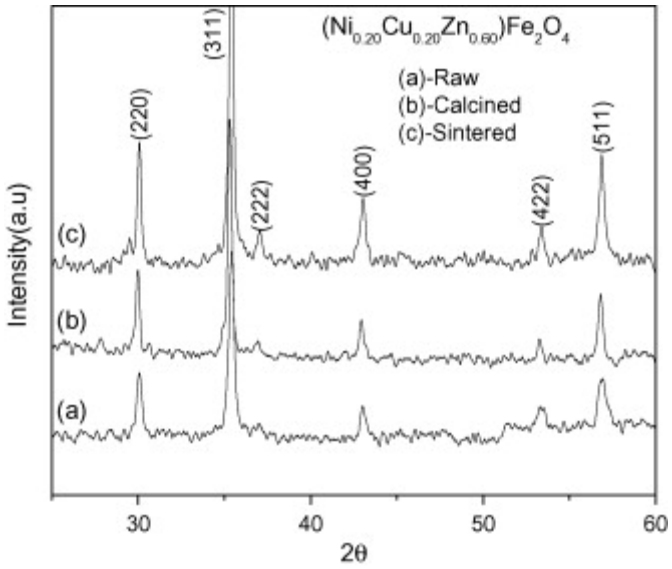

Fig. 3. XRD patterns of as-burnt, calcined and sintered $Ni_{0.2}Cu_{0.2}Zn_{0.6}Fe_2O_4$ ferrite.

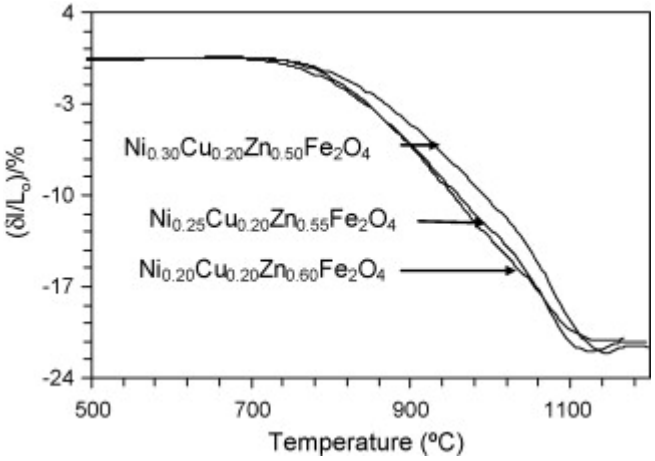

Fig. 4. Shrinkage curve at 5 °C/min heating rate in air for $Ni_{0.8-x}Cu_{0.2}Zn_xFe_2O_4$ ferrite with different Zn(x) content.

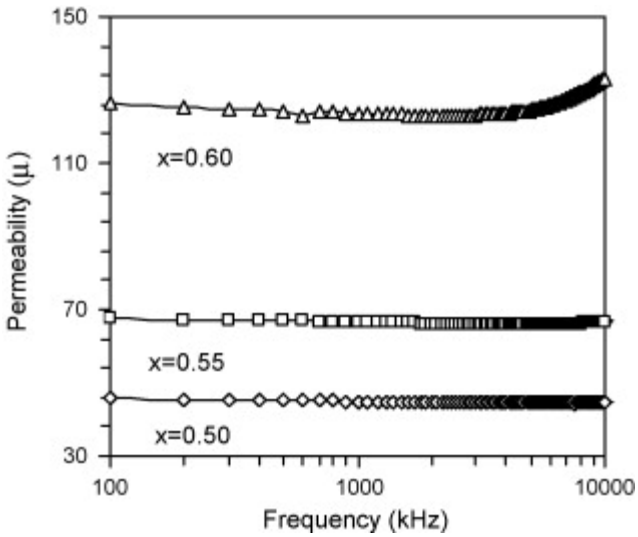

Fig. 5. Frequency dependency of permeability in $Ni_{0.8-x}Cu_{0.2}Zn_{xs}Fe_2O_4$ ferrite with different Zn(x) content.

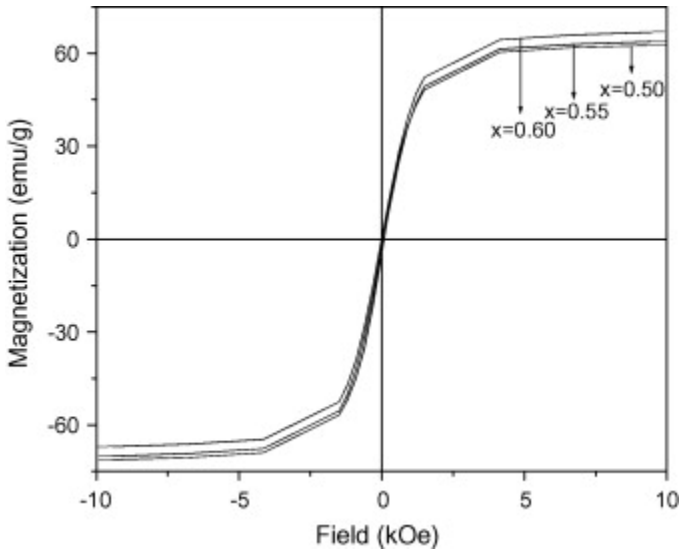

Fig. 6. Magnetic hysteresis curve for $Ni_{0.8-x}Cu_{0.2}Zn_xFe_2O_4$ ferrite with different Zn(x) content measured by VSM at 20 kOe and room temperature.

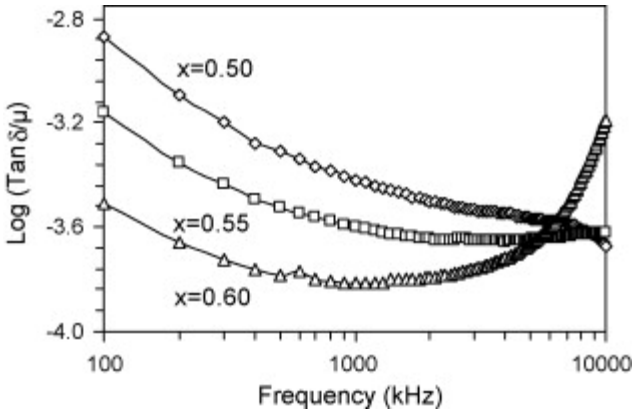

Fig. 7. Relative loss factor as a function of frequency in $Ni_{0.8-x}Cu_{0.2}Zn_xFe_2O_4$ ferrite with different Zn(x) content.

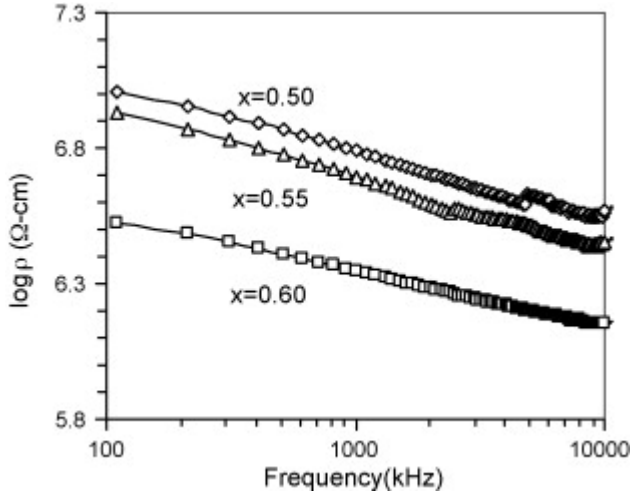

Fig. 8. ac resistivity as a function of frequency in $Ni_{0.8-x}Cu_{0.2}Zn_xFe_2O_4$ ferrite with different Zn(x) content.